Synthesis and mesomorphic behaviour of novel light-emitting liquid crystals

Matthew P. Aldred[a]; Amanda J. Eastwood[a]; Stuart P. Kitney[a]; Gary J. Richards[a]; Panos Vlachos[b]; Stephen M. Kelly[a]; Mary O'Neill[c]

[a] Department of Chemistry, University of Hull, Hull, UK [b] ZLX Techno Ltd., East Yorks, UK [c] Department of Physics, University of Hull, Hull, UK

PLEASE SCROLL DOWN FOR ARTICLE

Synthesis and mesomorphic behaviour of novel light-emitting liquid crystals

MATTHEW P. ALDRED†, AMANDA J. EASTWOOD†, STUART P. KITNEY†, GARY J. RICHARDS†, PANOS VLACHOS§, STEPHEN M. KELLY*† and MARY O'NEILL‡

†Department of Chemistry, University of Hull, Cottingham Rd., Hull, HU6 7RX, UK
‡Department of Physics, University of Hull, Cottingham Rd., Hull, HU6 7RX, UK
§ZLX Techno Ltd., 3 Trinity Lane, Beverley, East Yorks, HU17 ODY, UK

We report the results of a systematic study of the structure–mesomorphic behaviour relationships of a diverse range of light-emitting liquid crystals, but especially nematic 2,7-disubstituted-9,9-dialkylfluorenes. The dependence of the mesomorphic behaviour and transition temperatures on the nature and length of the terminal chains, the nature, position and number of lateral substituents and the number and nature of aromatic rings with and without heteroatoms in the central core is studied. The results of these studies are used to design polymerizable, light-emitting crystals (reactive mesogens) with a nematic phase having a high clearing point and a melting point below room temperature for facile OLED fabrication.

1. Introduction

The fabrication of solution-processable, red-green-blue pixellated organic light-emitting diodes OLEDs is not far from commercial realization using insoluble films of light-emitting and/or charge-transporting polymer networks [1–9]. A promising approach uses liquid crystalline polymer networks formed from polymerizable light-emitting liquid crystals — reactive mesogens (RMs) [2–9]. Light-emitting and charge-transporting RMs can be photolithographically patterned, often without a photoinitiator, to fabricate solution-processable, multilayer OLEDs with small, well resolved pixels [4–9]. The light-emitting devices reported so far using this approach have used light-emitting and/or charge-transporting polymer networks formed by polymerizing *discotic* or *nematic* monomers [3–15]. The short and long range order present in the layered structure of highly ordered smectic phases or 'plastic crystals' leads to a high charge carrier mobility [16–21]. For this reason a small number of smectic RMs have been prepared for use as charge carrying organic semiconductors with applications in Organic Field Effect Transistors (OFETs) as well as OLEDs [21–25]. We have demonstrated recently that OLEDs using smectic polymer networks are less efficient than the corresponding OLEDs using nematic liquid crystals [26].

*Corresponding author. Email: S.M.Kelly@hull.ac.uk

Therefore, we will concentrate in this report primarily on nematic liquid crystals.

Non-polymerizable nematic liquid crystals can also be used in OLEDs as long as they form a glassy LC state above room temperature, as do many reactive mesogens [7, 27–30]. The glass transition temperature should be considerably higher than room temperature to avoid crystallization during device operation. Non-polymerizable chiral nematic compounds in the glassy state can be used as organic lasers or to provide circularly polarized emission [31–33]. Since light-emitting and charge-transporting nematics can be used in OLEDs in the glassy, non-polymerizable form as well as crosslinked monomers, a more detailed investigation of structure–property relationships of nematic semiconductors is warranted as a future guide to designing and synthesizing optimized nematic semiconductors for OLEDs. Therefore, in this paper we report the synthesis, characterization and mesomorphic behaviour of a variety of non-polymerizable nematic, light-emitting liquid crystals, which can be used themselves or serve as models for reactive mesogens.

In designing nematic liquid crystalline materials for electronic/optoelectronic applications, the following structural features should be considered. Firstly, the aromatic core should have a large length-to-breadth ratio to induce liquid crystallinity. The core should be aromatic and have sufficient π-electron conjugation to result in appropriate HOMO and LUMO levels, that

determine the colour of emission, influence the charge mobility and control OLED efficiency [4–7]. A degree of molecular planarity with little inter-annular twisting will contribute to a high charge carrier mobility. The nature, number and position of heteroatoms in the aromatic core will influence the ionization potential and the electron affinity of these liquid crystalline semiconductors. Thirdly, melting points should be low, preferably close to, or at, room temperature to allow straightforward processing of the material. Therefore, long aliphatic chains in terminal and sometimes lateral positions should be present to reduce the van der Waals forces of attraction between the aromatic cores and to increase the intermolecular distance. Other substituents in lateral positions, such as fluorine, can achieve the same effect. However, these requirements are often mutually exclusive and a delicate balance of parameters is required that justifies the studies of structure/property relationships described in this manuscript.

2. Experimental

2.1. *Characterization*

For compounds with $RMM < 800\,g\,mol^{-1}$ mass spectra were recorded using a gas chromatography/mass spectrometer (GC/MS)-QP5050A Schimadzu with electron impact (EI) at a source temperature of $200^{\circ}C$. For compounds with $RMM > 800\,g\,mol^{-1}$ mass spectra were analysed using a Bruker, reflex IV, matrix assisted laser desorption/ionisation (MALDI), time of flight (TOF) MS. A 384-well microlitre plate format was used with a scout target. Samples were dissolved in DCM with 2-(4-hydroxyphenylazo)benzoic acid (HABA) matrix (1:10 respectively). IR spectra were recorded using a

Perkin-Elmer Paragon 1000 Fourier transform infrared (FTIR) spectrometer. ^1H NMR spectra were recorded using a JEOL Lambda 400 spectrometer and an internal standard of tetramethylsilane (TMS) was used. Aluminium-backed TLC plates coated with silica gel (60 F_{254} Merck) were used to measure the progress of reactions. GC was carried out using a Chromopack CP3800 gas chromatogaph equipped with a 10 m CP-SIL 5CB column. Purification of intermediates and final products was mainly accomplished by gravity column chromatography, using silica gel (40–63 microns, 60 A) obtained from Fluorochem. The melting point and liquid crystal transition temperatures of the prepared solids were measured using a Linkam 350 hot stage and control unit in conjunction with a Nikon E400 polarizing microscope. The transition temperatures of all the final products were confirmed using a Perkin-Elmer DSC-7 in conjunction with a TAC 7/3 instrument controller, using the peak measurement for the reported value of the transition temperatures. Half Cp extrapolated was used to measure the glass transition temperature (T_g). Thin layer chromatography (TLC), GC and elemental analysis, using a Fisons EA 1108 CHN system, were employed to measure the purity of intermediates and final compounds.

The thermotropic mesophases observed for the materials collated in tables 1–9 were investigated between cross polarizers using optical microscopy. Only the nematic phase (N), the chiral nematic phase (N*), the chiral smectic A phase (SmA*) and the chiral smectic C phase (SmC*) were observed. Typically, nematic droplets were observed on slow cooling from the isotropic liquid, see figure 1. Figure 2 shows the Schlieren texture, typically observed for most of the
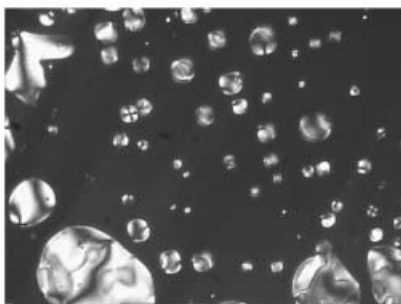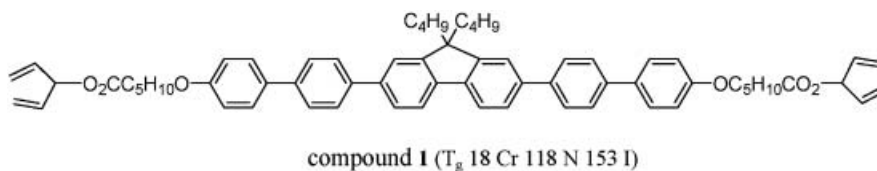

compound **1** (T$_g$ 18 Cr 118 N 153 I)

Figure 1. Droplet texture of compound **1**, formed by slow cooling ($1^{\circ}C\,min^{-1}$) from the clearing point to the onset of the nematic phase.
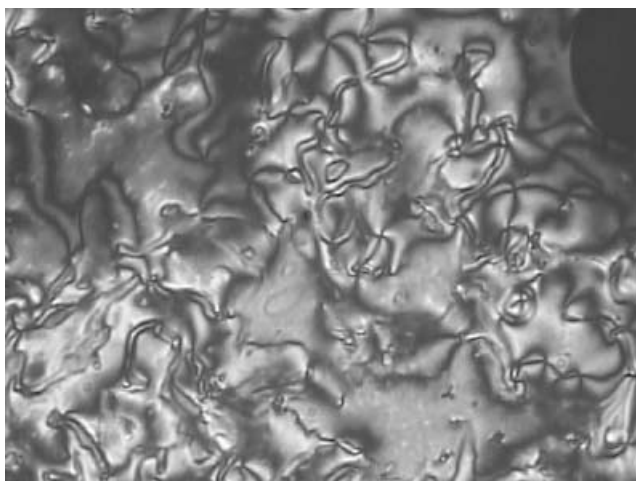
Figure 2. The schlieren texture of the nematic phase of compound **1** at 135°C.

compounds, with two- and four-point brushes, which is characteristic of a nematic phase. The smectic A phase exhibited the focal conic texture as well as optically extinct areas in the same sample. The simultaneous presence of these two textures is typical of the calamitc smectic A phase or its chiral equivalent. The elliptical and hyperbolic lines of optical discontinuity characteristic of

focal conic defects were also observed. The focal conics develop dark bars across their backs on cooling into the smectic C phase and isotropic areas show a schlieren texture with only four point brushes at this transition.

The transition temperatures observed using optical microscopy were confirmed by differential scanning calorimetry (DSC). For example, the DSC trace shown in figure 3 confirms the liquid crystalline transition temperatures of compound **1**. The baseline of the spectra is relatively flat and sharp transition peaks are observed with no thermal degradation. The large melting transition peak and the relatively small nematic–isotropic peak is characteristic of a nematic liquid crystal. A second order transition peak is observed on cooling and heating at 18°C, which is characteristic of a glass transition temperature due to a shift in the baseline. Crystallization occurs at 31°C on heating above the glass transition temperature. Although compound **1** has a low T_g, no crystallization is observed when a thin film is left in ambient conditions over a long period of time, even after 6 months. The enthalpies of transition for the smectic A and smectic C phases exhibit intermediate values between the high value for the melting point and the low value for the N–I transition.
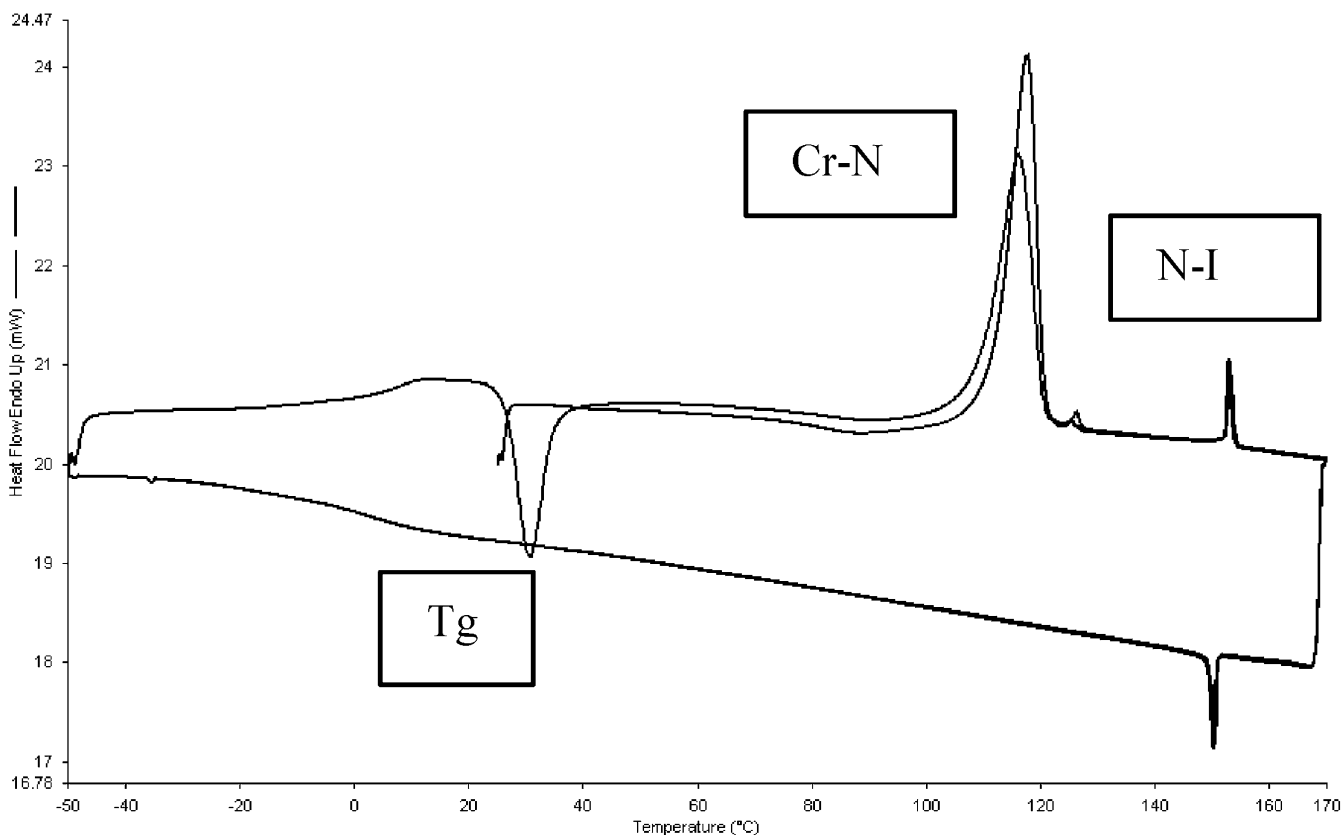

Figure 3. DSC scan as a function of temperature for compound **1** at a scan rate of $10°C\,min^{-1}$.

2.2. *Synthesis*

All commercially available starting materials, reagents and solvents were used as supplied, unless otherwise stated, and were obtained from Aldrich, Strem Chem. Inc., Acros or Lancaster Synthesis. Tetrahydrofuran was pre-dried with sodium wire and then distilled over sodium wire under nitrogen with benzophenone indicator, when required and was not stored. All reactions were carried out using a dry nitrogen atmosphere unless water was present as solvent or reagent and the temperatures were measured externally.

2.2.1. 4-Bromo-2-fluoro-1-octyloxybenzene.
A mixture of 4-bromo-2-fluorophenol (50.0 g, 0.2618 mol), 1-bromooctane (60.6 g, 0.3141 mol) and potassium carbonate (72.3 g, 0.5236 mol) in butanone (500 cm^3) was heated under reflux overnight. The cooled reaction mixture was filtered and the filtrate concentrated under reduced pressure. The crude product was distilled to yield a colourless oil (63.2 g, 79.7%), b.p. 146–150°C @ 1 mbar Hg, purity >99% (GC), ^{1}H NMR (CDCl$_3$) δ_H: 0.88 (3H, t), 1.22–1.39 (8H, m), 1.45 (2H, quint), 1.80 (2H, quint) 3.99 (2H, t), 6.80 (1H, overlapping dd, J=8.7 Hz), 7.15 (1H, ddd, J=1.1, 2.3, 8.7 Hz), 7.21 (1H, dd, J=2.3, 10.7 Hz). IR v_{max}/cm^{-1}: 3079, 2952, 2928, 2856, 1583, 1505, 1469, 1305, 1266, 1208, 1131, 1070, 1021, 875, 799. MS m/z (EI): 304, 302 (M$^+$), 231, 192 (M100), 190, 163, 161, 142, 111, 94, 83, 69. Combustion analysis: expected C 55.46, H 6.65; obtained C 55.62, H 6.55%.

2.2.2. 3-Fluoro-4-octyloxyphenyl boronic acid.
A solution of *n*-BuLi in hexanes (75.9 cm^3, 2.5M, 0.1898 mol) was added dropwise to a cooled (−78°C) solution of 4-bromo-2-fluoro-1-octyloxybenzene (50.0 g, 0.1650 mol) in THF (dry, 400 cm^3). The resultant solution was stirred at this temperature for 1 h and then trimethyl borate (34.3 g, 0.3300 mol) was added dropwise. After completion of the addition the reaction mixture was allowed to reach r.t. and stirred overnight. Hydrochloric acid (20%, 200 cm^3) was added and the resultant mixture stirred for 1 h and then extracted into diethyl ether (2 × 300 cm^3). The combined ethereal extracts were washed with water (2 × 150 cm^3) and dried (MgSO$_4$). After filtration the solvent was removed under reduced pressure. The crude product was not purified (35.0 g, 79.2%), m.p. 115°C. ^{1}H NMR ((CD$_3$)$_2$SO) δ_H: 0.84 (3H, t), 1.20–1.33 (8H, m), 1.38 (2H, quint), 1.72 (2H, quint) 4.01 (2H, t), 6.87–6.91 (1H, m), 7.06–7.16 (1H, m), 7.50–7.55 (1H, m), 8.00 (2H, s, –OH). IR v_{max}/cm^{-1}: 3200–3450, 3069, 2950, 2933, 2856, 1583, 1504, 1469, 1330, 1305, 1261, 1208, 1131, 1070, 1021, 870, 798. MS m/z (EI): 268 (M$^+$), 240, 224, 206, 190, 149, 128, 112 (M100), 95, 83, 69.

2.2.3. 4-Bromo-3′-fluoro-4′-octyloxybiphenyl.
Tetrakis-(triphenylphosphine)palladium(0) (3.23 g, 2.80 × 10^{-3} mol) was added to a stirred solution of 3-fluoro-4-octyloxyphenyl boronic acid (15.0 g, 0.0560 mol), 1-bromo-4-iodobenzene (17.4 g, 0.0616 mol) and a 20% aqueous sodium carbonate solution (120 cm^3) in 1,4-dioxane (500 cm^3) at r.t. The reaction mixture was heated under reflux overnight. The cooled reaction mixture was added to water (150 cm^3) and the product extracted into diethyl ether (2 × 300 cm^3). The combined ethereal extracts were washed with hydrochloric acid (10%, 50 cm^3), water (2 × 100 cm^3), dried (MgSO$_4$), filtered and concentrated under reduced pressure. The crude product was purified by gravity column chromatography (DCM/hexane, 10/90) to yield a white powder (10.00 g, 47.2%), m.p. 35–37°C. ^{1}H NMR (CDCl$_3$) δ_H: 0.88 (3H, t), 1.24–1.40 (8H, m), 1.48 (2H, quint) 1.83 (2H, quint), 4.06 (2H, t), 7.01 (1H, overlapping dd, J=8.7 Hz), 7.24 (1H, ddd, J=1.1, 2.3, 8.4 Hz), 7.28 (1H, dd, J=2.3, 12.4 Hz), 7.38 (2H, d, J=8.7 Hz), 7.53 (2H, d, J=8.7 Hz). IR v_{max}/cm^{-1}: 3055, 2964, 2920, 2853, 1610, 1553, 1536, 1510, 1469, 1275, 1136, 1121, 869, 831, 810. MS m/z (EI): 380, 378 (M$^+$), 300, 268, 266 (M100), 188, 172, 170, 139, 112, 97, 83, 69. Combustion analysis: expected C 63.33, H 6.38; obtained C 63.53, H 6.63%.

2.2.4. 3-Fluoro-4-octyloxybiphenyl-4′-yl boronic acid.
A solution of *n*-BuLi in hexanes (17.7 cm^3, 2.5M, 0.0443 mol) was added dropwise to a cooled (−78°C) solution of 4-bromo-3′-fluoro-4′-octyloxybiphenyl (14.6 g, 0.0385 mol) in THF (dry, 200 cm^3). The resultant solution was stirred at this temperature for 1 h and then trimethyl borate (12.0 g, 0.1156 mol) was added dropwise. After completion of the addition the reaction mixture was allowed to reach r.t. and stirred overnight. Hydrochloric acid (20%, 100 cm^3) was added and the mixture stirred for 1 h and then extracted into diethyl ether (2 × 250 cm^3). The combined ethereal extracts were washed with water (2 × 150 cm^3) and dried (MgSO$_4$). After filtration the solvent was removed under reduced pressure. The crude product was purified by stirring with hexane (5 min) and filtering to yield a white powder (7.33 g, 55.1%), m.p. 120–122°C. ^{1}H NMR ((CD$_3$)$_2$SO) δ_H: 0.86 (3H, t), 1.22–1.38 (8H, m), 1.46 (2H, quint), 1.74 (2H, quint) 4.08 (2H, t), 7.23 (1H, overlapping dd, J=9 Hz), 7.46–7.49 (1H, m), 7.57 (1H, dd, J=2.2, 13 Hz), 7.61 (2H, d, J=8.1 Hz), 7.84 (2H, d, J=8.1 Hz), 8.07 (2H, s, –OH). IR v_{max}/cm^{-1}: 3100–3500, 3065, 2960, 2923, 2853, 1606, 1553, 1536, 1511, 1469, 1277, 1136, 1120, 874, 835, 809. MS m/z (EI): no mass ion. Combustion analysis: expected C 69.78, H 7.61; obtained C 69.39, H 7.86%.

2.2.5. 2,7-Bis(3-fluoro-4-octyloxybiphenyl-4′-yl)-9,9-dioctylfluorene (25).

Tetrakis(triphenylphosphine)-palladium(0) (0.95 g, 8.21×10^{-4} mol) was added to a stirred solution of 3-fluoro-4-octyloxybiphenyl-4′-yl boronic acid (7.04 g, 0.0205 mol), 2,7-dibromo-9,9-dioctylfluorene (24) (4.50 g, 0.0082 mol) and 20% aqueous sodium carbonate (12.5 cm^3) in DME (150 cm^3) at r.t. The reaction mixture was heated under reflux for 24 h; after cooling it was added to water (150 cm^3) and the product extracted into DCM (2 × 200 cm^3). The combined organic layers were washed with hydrochloric acid (10%, 50 cm^3), water (2 × 100 cm^3), dried (MgSO$_4$), filtered and concentrated under reduced pressure. Catalyst residues were removed by passing the crude product though a short column containing silica gel (DCM/hexane, 50/50). The product was recrystallized from a DCM and ethanol mixture to yield a yellow–white crystalline solid (5.15 g, 63.6%), transition temp. g-7 Cr 101 N 117 I(°C). ^{1}H NMR (CDCl$_3$) δ_H: 0.74 (4H, quint), 0.79 (6H, t), 0.90 (6H, t), 1.00–1.24 (20H, m), 1.25–1.42 (16H, m), 1.50 (4H, quint), 1.86 (4H, quint), 2.04–2.08 (4H, m), 4.09 (4H, t), 7.05 (2H, overlapping dd, $J=8.4$ Hz), 7.34–7.37 (2H, m), 7.40 (2H, dd, $J=2.0$, 12.4 Hz), 7.60–7.63 (4H, m), 7.64 (4H, d, $J=8.2$ Hz), 7.74 (4H, d, $J=8.2$ Hz), 7.79 (2H, d, $J=7.9$ Hz). IR v_{max}/cm^{-1}: 3095, 3038, 2925, 2856, 1610, 1584, 1527, 1499, 1467, 1289, 1250, 1182, 1146, 1046, 867, 812. MS m/z (MALDI): 987 (M$^+$). Combustion analysis: expected C 83.93, H 8.98; obtained C 83.64, H 9.24%.

2.2.6. 2,7-Bis(3-fluoro-4-hydroxybiphenyl-4′-yl)-9,9-dioctylfluorene.

Boron tribromide (1.38 cm^3, 0.0146 mol) in DCM (10 cm^3) was added dropwise to a cooled (0°C) stirred solution of 2,7-bis(3-fluoro-4-octyloxybiphenyl-4′-yl)-9,9-dioctylfluorene (4.80 g, 0.0049 mol) in chloroform (80 cm^3). The reaction mixture was stirred at r.t. overnight, then poured onto an ice/water mixture (200 g) and stirred for 30 min. The product was extracted into ethyl acetate (2 × 150 cm^3). The combined organic layers were washed with water (2 × 100 cm^3), dried (MgSO$_4$), filtered and concentrated under reduced pressure. The crude product was purified by gravity column chromatography (silica gel, ethyl acetate/hexane, 30/70) to yield a white crystalline solid (2.70 g, 72.8%), m.p. 130°C. ^{1}H NMR (CDCl$_3$) δ_H: 0.75 (4H, quint), 0.79 (6H, t), 1.02–1.20 (20H, m), 2.04–2.08 (4H, m), 5.20 (2H, d, –OH), 7.10 (2H, overlapping dd, $J=8.4$ Hz), 7.34–7.36 (2H, m), 7.40 (2H, dd, $J=2.0$, 12.4 Hz), 7.60–7.63 (4H, m), 7.64 (4H, d, $J=8.2$ Hz), 7.74 (4H, d, $J=8.2$ Hz), 7.79 (2H, d, $J=7.9$ Hz). IR v_{max}/cm^{-1}: 3100–3500, 3030, 2954, 2926, 2853, 1622, 1599,

1532, 1506, 1465, 1279, 1238, 1168, 1113, 873, 812. MS m/z (MALDI): 763 (M$^+$). Combustion analysis: expected C 83.43, H 7.40, obtained C 83.21, H 7.56%.

2.2.7. 2,7-Bis{3-fluoro-4-[(S)-3,7-dimethyloct-6-enyloxy]-biphenyl-4′-yl}-9,9-dioctylfluorene (30).

A mixture of 2,7-bis(3-fluoro-4-hydroxybiphenyl-4′-yl)-9,9-dioctylfluorene (0.30 g, 3.93×10^{-4} mol), (S)-(+)-citronellyl bromide (0.26 g, 0.0012 mol) and potassium carbonate (0.16 g, 0.0012 mol) in DMF (20 cm^3) was heated at 90°C for 48 h. The reaction mixture was cooled to r.t., water (50 cm^3) was added and the product extracted into DCM (2 × 100 cm^3). The combined organic layers were washed with brine (4 × 100 cm^3), dried (MgSO$_4$), filtered and concentrated under reduced pressure. The crude product was purified by gravity column chromatography (silica gel, DCM) and recrystallized from a DCM and ethanol mixture to yield a white solid (0.17 g, 41.5%), transition temp. Cr 82 N* 69 I(°C). ^{1}H NMR (CDCl$_3$) δ_H: 0.74 (4H, quint), 0.79 (6H, t), 0.98 (6H, d), 1.02–1.20 (20H, m), 1.16–1.47 (4H, m), 1.53–1.60 (4H, m), 1.62 (6H, s), 1.70 (6H, s), 1.83–1.92 (2H, m), 1.99–2.08 (8H, m), 4.08–4.16 (4H, m), 5.12 (2H, t), 7.06 (2H, overlapping dd, $J=8.4$ Hz), 7.35–7.37 (2H, m), 7.39 (2H, dd, $J=2.3$, 12.4 Hz), 7.60–7.63 (4H, m), 7.65 (4H, d, $J=8.4$ Hz), 7.75 (4H, d, $J=8.4$ Hz), 7.79 (2H, d, $J=7.9$ Hz). IR v_{max}/cm^{-1}:3076, 2936, 2857, 1737, 1710, 1600, 1545, 1500, 1462, 1376, 1291, 1271, 1254, 1179, 1004, 864, 829, 800. MS m/z (MALDI): 1039 (M$^+$). Combustion analysis: expected C 84.35, H 8.92; obtained C 84.31, H 9.23%.

3. Results and discussion

3.1. Syntheses

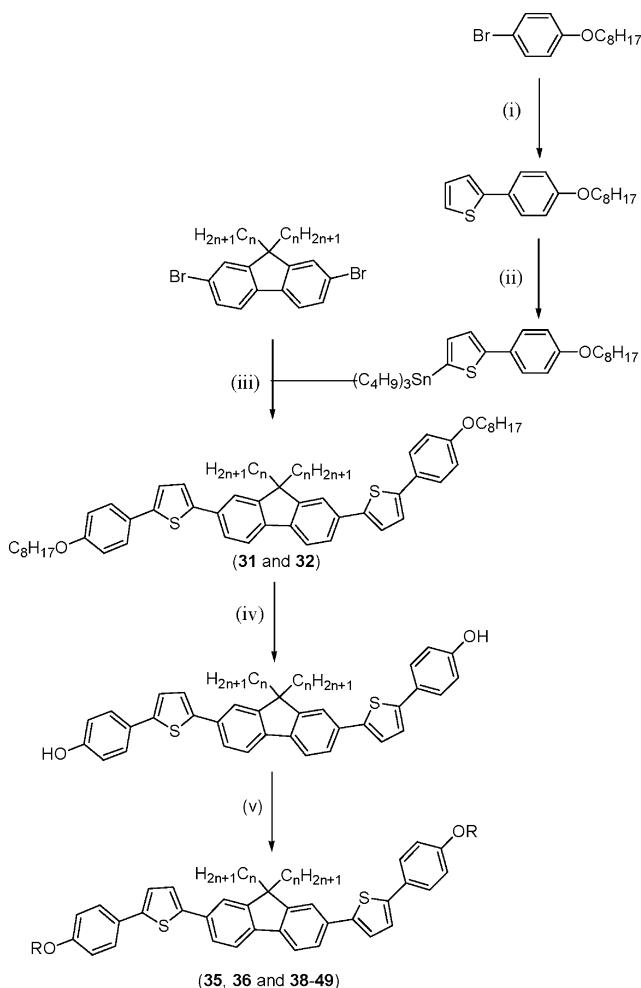The general methods of synthesis of the thiadiazoles, pyridines, pyrimidines and benzothiadiazoles 2–10, 16 and 17 and the fluorenes 1, 11–15, 18–30 have been described elsewhere. [14, 15, 20, 25, 26]. Compounds 25 and 30 were synthesised according to the reaction scheme 1. The boronic acid formed from the ether-protected 4-bromo-2-fluorophenol was used in a selective Suzuki crosscoupling [34] reaction with 1-bromo-4-iodobenzene to afford 4-bromo-3′-fluoro-4′-octyloxybiphenyl. This was converted to the boronic acid as usual and reacted with 2,7-dibromo-9,9-dioctylfluorene in a Suzuki crosscoupling reaction to afford the hexaphenylene 25. The corresponding diphenol was produced by ether cleavage using boron tribromide [35] and used in a subsequent Williamson-ether alkylation [36] with (S)-(+)-citronellyl bromide to yield compound 30. Compound 26 was synthesized in a similar manner to compound 25. However 3′-fluoro-4-octyloxybiphenyl-4′-yl boronic acid
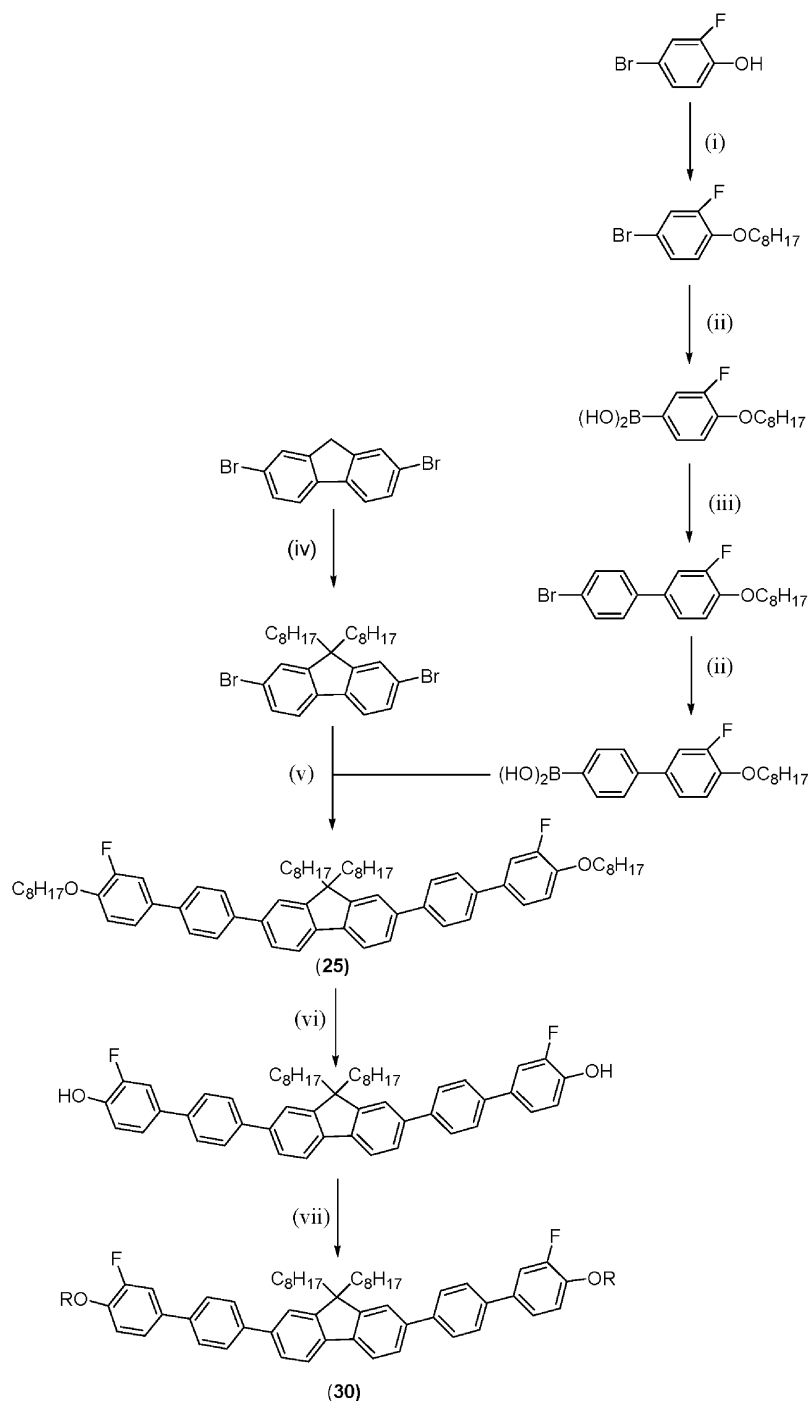
Scheme 1. Reagents and conditions: (i) BrC_8H_{17}, K_2CO_3, butanone, reflux; (ii) (a) *n*-BuLi, THF, $-78^\circ C$, (b) $B(OMe)_3$, (c) H_3O^+; (iii) 1-bromo-4-iodobenzene, Na_2CO_3 (aq), $Pd(PPh_3)_4$, DME, reflux; (iv) tributylammonium bromide (TBAB), 50% $NaOH_{(aq)}$, 1-bromooctane, toluene, reflux; (v) Na_2CO_3 (aq), $Pd(PPh_3)_4$, DME; (vi) (a) BBr_3, CH_2Cl_2, $0^\circ C$, (b) H_2O (ice); (vii) *R*Br, K_2CO_3, DMF, $90^\circ C$.

was used in the Suzuki crosscoupling reaction with 2,7-dibromo-9,9-dioctylfluorene, which was prepared by alkylation of fluorene in one step followed by

bromination using a solution of bromine in chloroform [14, 15]. The general synthetic route used to obtain the thiophene-based fluorenes **31**, **32**, **35–36** and **38–49** is

3.2. *Mesomorphic behaviour*

The transition temperatures for a diverse range of heterocyclic compounds (**2**–**10**) are collated in table 1. Only three examples of the three-ring compounds **2**–**7** exhibit liquid crystalline phases (SmA* and SmC*). The benzothiazole **3** with a fluorine atom in position 3 of each of the 1,4-disubstituted phenyl rings exhibits a monotropic chiral smectic A* phase. The melting point of benzothiazole **3** is lower than that of the corresponding non-fluoro-substituted compound **2**. The benzothiadiazole **4** also contains two thiophene rings in the aromatic core. The low melting point below room temperature and the absence of an observable liquid crystalline phase of the benzothiadiazole **4** are probably attributable to the non-coaxial nature of the 2,5-disubtituted thiophene bonds (angle 148°, i.e. a 32° deviation from linearity). The pyridine **5** exhibits similar transition temperatures to those of the corresponding pyrimidine **6**, except for a smectic A* phase above the chiral smectic C* phase exhibited by both compounds. The pyrimidine **7** with a fluorine atom in position 3 of each 1,4-disubstituted phenyl ring is not mesomorphic. The melting point is higher than that of the corresponding non-fluoro-substituted analogue **6**, and a monotropic phase could not be observed below the melting point for compound **7**. This shows how difficult it is to predict with certainty the effect of a particular functional group on the transition temperatures of the molecule containing it, although trends are often general. An example of this latter point is the fact that compounds **8**–**10** with four aromatic rings in the aromatic core exhibit a greater tendency for mesophase formation and higher clearing points than those analogues with only three rings in the core.

The effect of the presence of one or two alkyl substituents in position 9 of the fluorene moiety and on the transition temperatures of some low molar mass liquid crystals (**11**–**17**) is demonstrated in tables 2 and 3. Most of the liquid crystalline 9,9-dialkylpolyfluorenes [38–40], oligofluorenes [27–30] and small molecules [14, 15], similar in general structure to those in the tables 2 and 3, which have been reported so far in the literature, exhibit a nematic phase, rather than a smectic phase. This is because the alkyl chains in the 9-position prevent formation of the layer structure of smectic phases. The two alkyl chains are constrained orthogonal to the fluorene unit [41] as a consequence of *sp3* bonding, and as such they act as large lateral substituents. These are known to lead generally to low liquid crystalline temperatures and the suppression of smectic phases due to the induction of large intermolecular distances and low intermolecular forces of attraction, such as van der Waals interactions [14, 15]. This steric effect is also

Scheme 2. Reagents and conditions: (i) 2-(tributylstannyl)thiophene, Pd(PPh$_3$)$_4$, DMF, 90°C; (ii) (a) *n*-BuLi, THF, −78°C, (b) Sn(C$_4$H$_9$)$_3$Cl; (iii) Pd(PPh$_3$)$_4$, DMF, 90°C; (iv) (a) BBr$_3$, CH$_2$Cl$_2$, 0°C, (b) H$_2$O (ice); (v) *R*Br, K$_2$CO$_3$, DMF, 90°C.

shown in scheme 2. An initial Stille coupling [37] between 2-tributylstannylthiophene and 1-bromo-4-octyloxybenzene afforded 2-(4-octyloxyphenyl)thiophene, lithiation of which using *n*-BuLi followed by quenching with tributyltin chloride gave the corresponding tin reagent, which was used without further purification due to its susceptibility to destannylation. Another Pd-catalysed Stille coupling, involving 2,7-dibromo-9,9-dipropyl(octyl)fluorene and the tin reagent gave materials **31** and **32**. Deprotection, using BBr$_3$ in DCM, and subsequent Williamson-ether alkylations with the appropriate 1-bromoalkane gave the desired compounds **35**, **36** and **38**–**49**. The lateral substituted methyl derivatives **50**–**52**, (shown in table 8), were synthesized in a similar manner using commercially available 4-bromo-3-methylanisole, 4-bromo-2,6-dimethylanisole and 4-bromo-2-methylanisole.
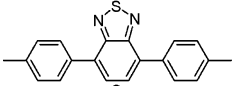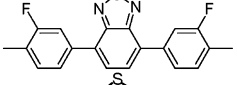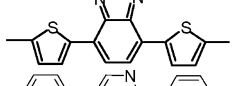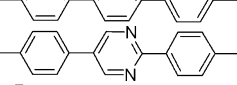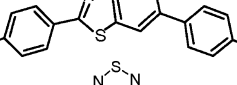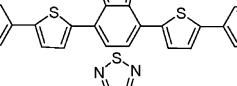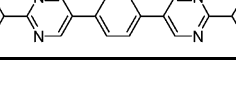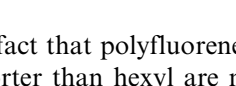
Table 1. Transition temperatures (°C) for the heterocyclic compounds **2**–**10**.

Compound	Core	Cr		SmC*		SmA*		I
2		•	95		—		—	•
3		•	64		—	(•	55)	•
4		•	<25		—		—	•
5		•	83	•	102	•	128	•
6		•	86	•	104		—	•
7		•	115		—		—	•
8		•	79	•	114		—	•
9		•	152		—	•	199	•
10		•	155		—	•	302	•

revealed by the fact that polyfluorenes that incorporate alkyl chains shorter than hexyl are not very soluble in most organic solvents due to high intermolecular van der Waals forces of attraction [38]. It has also been reported that smectic phases can still be obtained for ter-fluorene-based compounds when the alkyl chains are very short, i.e. methyl chains are incorporated at the 9-position, rather than longer alkyl chains [42]. Therefore, it is not surprising that the compounds **11**–**16** exhibit only a chiral nematic phase and not smectic phases. The melting and clearing points of the compounds **11** and **13** with one alkyl group at position 9 are higher than those of the corresponding compounds **12** and **14** with two alkyl chains in the same position. This is consistent with the above explanations. Hence, the presence of two fluorene units in compound **15** leads to a lower clearing point than that of compound **14** with the same molecular length but only one fluorene unit. The presence of four 2,5-disubstituted thiophene rings in compounds **16** and **17**, shown in table 3, leads to a low tendency for mesophase formation and low clearing points for the reasons described above for compound **4**.

Taking into account the tendency for nematic phase formation and other advantageous properties of 2,7-disubstituted-9,9-dialkylfluorenes, led us to concentrate further studies on liquid crystals containing the fluorene unit as an essential part of the central chromophore. The results of our studies of the mesomorphic behaviour of smectic reactive mesogens are reported elsewhere [20, 25, 26]. The photoluminescence spectra of the compounds listed in table 1 indicate that the HOMO and LUMO energy levels, and hence the emission spectrum of these materials, can be modified by molecular engineering. For example, the PL emission of the pyrimidine **6** is blue, that of the benzothiadiazole **2** is green, but that of the benzothiadiazole **9** is red. This is dealt with elsewhere as the PL spectra of the smectic reactive mesogen analogues of the compounds listed in table 1 are almost identical to those of their non-polymerizable analogues reported here [20, 25, 26].

The compounds **18**–**26** listed in table 4 were synthesized in order to identify structure–property relationships, which would allow the melting point to be reduced as much as possible by varying the length of the alkyl chain at the 9-position on the fluorene moiety in

Table 2. Transition temperatures (°C) for the fluorenes **11–15**.

Compound	Core	g		Cr		N*		I
11		•	98	—		•	108	•
12		•	63	—		•	108	•
13				•	205	•	246	•
14				•	127	•	187	•
15			45	•	141	•	145	•

Table 3. Transition temperatures (°C) for the fluorene **16** and the benzothiadiazole **17**.

Compound	Core	g		Cr		N*		I
16		•	18	•	61	(•	32)[a]	•
17				•	133	—		•

[a]Parentheses represent a monotropic transition.

Table 4. Transition temperatures (°C) for the fluorenes **18–26**.

Compound	X	Y	n	g		Cr		N		I
18	H	H	2		—	•	146	•	290	•
19	H	H	3		—	•	157	•	232	•
20	H	H	4		—	•	156	•	216	•
21	H	H	5		—	•	139	•	200	•
22	H	H	6		—	•	123	•	188	•
23	H	H	8	•	−10	•	105	•	166	•
24	H	H	10	•	1	•	103	•	146	•
25	F	H	8	•	−7	•	101	•	117	•
26	H	F	8	•	−4	•	96	•	131	•

the centre of the molecule, i.e. by varying the number of carbon atoms in the chain, $n = 2$–10. The presence of two decyl chains in the fluorene **24** leads to a much lower melting point and clearing point compared with the corresponding compound **18** with the much shorter ethyl chain in place of the decyl chain, for example. The melting and clearing points decrease as the homologous series **18**–**24** is ascended, although the clearing point is reduced to a greater degree than the melting point. This can be attributed to the steric effects and weaker van der Waals forces between the molecules, as described above, as the longer chains increase the intermolecular distance [15, 27–30, 38, 39]. An odd–even effect in the nematic clearing point is observed as expected.

The incorporation of fluorine atoms in a lateral position of the aromatic cores of liquid crystals often reduces the melting points due to the same steric effects referred to above [43]. This effect is demonstrated in the fluorenes **25** and **26**. The lower melting point of compounds **25** and **26**, compared with that of the non-fluoro-substituted analogue **23**, is also probably attributable to steric effects. The lower melting point of compound **26** compared with compound **25**, is also probably due to the occurrence of significant inter-annular twisting between the biphenyl units of compound **26**. The hydrogen and fluorine atoms *ortho* to the ring junction are constrained away from each other, which increases the dihedral angles and subsequently decreases the degree of polarizability between the π-systems of each aromatic ring, compared with the analogous compounds **23** and **25**. Therefore the packing of the molecules in compound **26** is likely to be less efficient than to that in compounds **23** and **25**, and consequently the melting point is lower for compound

26. The clearing points of compounds **25** and **26** are also lower than the clearing point of compound **23**, which is probably due to similar effects as expected.

The fluorenes with shorter alkyl chain lengths **18**–**22** do not possess a glass transition temperature, whereas compounds **23**–**26** exhibit a glass transition temperature below $0°C$. This observation is consistent with the observation that vitrification requires a very high viscosity. In accordance to the Tammann rule [44], any compounds can become glassy if it can be cooled below the glass transition temperature without crystallization. Crystallization on cooling below the melting point (supercooling) is inhibited if the viscosity of the molecule is very high. Long alkyl chains can give rise to a high viscosity of a compound, hence the occurrence of glass transitions in compounds **23**–**26**. Also the larger substituents render the central portion of the aromatic molecular core effectively more bulky, providing effective steric hindrance to close inter-molecular packing, which will also inhibit crystallization [45]. The efficacy of the molecular engineering demonstrated above in reducing the melting points can be appreciated by comparing the melting point of *para*-sexiphenyl ($465°C$), which is a rigid aromatic compound with six phenylene rings, with that ($96°C$) of the fluorene **26**.

A comparison of the transition temperatures shown in table 5 demonstrates the influence of branching in different side chain groups situated at the ends of the rigid aromatic core. The presence of a branching methyl group in the spacer between the aromatic core and the polymerizable end group in compound **28** leads to lower transition temperatures than those of the corresponding compound **27** with the same spacer length. This is also due to steric effects as described above. The same effect

Table 5. Transition temperatures ($°C$) for the fluorenes **23**, **25** and **27**–**30**.

Compound	X	R¹	t_g		Cr		N/N*		I
27	H		—	•	91	•	109	•	
28	H		—	•	76	•	82	•	
23	H		•	−10	•	105	•	166	•
29	H		—	•	97	•	132	•	
25	F		•	−7	•	101	•	117	•
30	F		—	•	82	(•	69)[a]	•	

[a]Parentheses denote a monotropic mesophase.

is also demonstrated on comparing the transition temperatures of compounds **23** and **29**, and comparing those of compounds **25** and **30**. In compound **30**, the clearing point is reduced to a much greater extent than the melting point, in comparison with compound **29**. Therefore it is not surprising that compound **30** is monotropic. Low glass transition temperatures or no glass transitions at all are observed for the compounds shown in table 5.
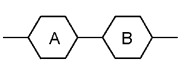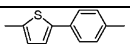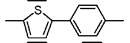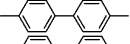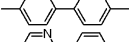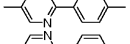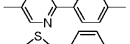
The fluorenes shown in table 6 contain either two thiophene or two pyrimidine rings, which have replaced the two phenylene rings that are incorporated in the related fluorenes mentioned above. The photopolymerizable analogue of the compounds shown in tables 4–6 exhibits good hole-transporting and electroluminescent properties. [4, 14, 15] Other non-polymerizable homologues were synthesized in order to optimize the liquid crystal transition temperatures and to facilitate the investigation of the influences of these structural changes on the mesomorphism of this type of compound.

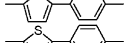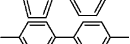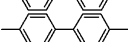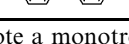The biphenyl-fluorenes **23**, **29** and **37** exhibit higher melting and clearing points as well as a broader nematic phase compared with those of the analogous thiophene-containing fluorenes **32**, **35** and **36** with the same terminal and lateral alkyl chains. These differences in transition temperatures may well be due to the lower length-to-breadth ratio of the thiophene-containing fluorenes **32**, **35** and **36**. The aromatic cores containing two thiophene rings give rise to a glass transition,

whereas no glass transition or a glass transition at low temperature, e.g. $-10°C$ for compound **23**, is observed when the two thiophene rings are replaced with two phenyl rings. Perhaps the non-colinear nature of the 2,5-disubstituted thiophene bonds contributes to a higher tendency for glass formation. The branched chain compounds **29** and **34–37**, which incorporate the (S)-(+)-citronellyl alkyl chain, exhibit lower melting and clearing points than the analogous *n*-octyl derivatives.

Compound **31** with a straight octyloxy chain serves as a model compound for comparisons of the compounds listed in table 7. The transition temperatures of the octenyloxy-substituted compound **38** are lower, as expected based on previous results [46]. The melting and clearing point of compounds **35** and **39–44** decrease with increasing length of the terminal branched alkoxy chain. This can be attributed to a normal dilution effect as the ratio of flexible aliphatic components of the molecular structure increases with respect to the rigid aromatic core. The melting and clearing points of the chiral octyl fluorene **36** are lower compared with the chiral propyl fluorene **35**, due to the occurrence of weaker van der Waals forces between the molecules. The effect on the melting point is comparable to the effect on the clearing point, and therefore the clearing point of compound **36** is not monotropic, in contrast to compound **35**. Fluorene **43** has a lower melting point than that ($-13°C$) of the corresponding compound **35**, where the only difference between the two compounds is the presence of an unsaturated bond. This may be due

Table 6. Transition temperatures (°C) for the fluorenes **19**, **23**, **29** and **31–37**.

Compound	structure (A–B)	R^1	R^2	g	Cr	N/N*	I
31	thiophene–phenyl	C_3H_7	*n*-octyl	• 30	• 169	(• 168)ᵃ	•
32	thiophene–phenyl	C_8H_{17}	*n*-octyl	• −12	• 69	• 99	•
19	phenyl–phenyl	C_3H_7	*n*-octyl	—	• 157	• 232	•
23	phenyl–phenyl	C_8H_{17}	*n*-octyl	• −10	• 105	• 166	•
33	pyrimidine–phenyl	C_3H_7	*n*-octyl	—	• 177	• 194	•
34	pyrimidine–phenyl	C_3H_7	(S)-(+)-citronellyl	• 18	• 113	• 120	•
35	thiophene–phenyl	C_3H_7	(S)-(+)-citronellyl	• 23	• 123	(• 122)	•
36	thiophene–phenyl	C_8H_{17}	(S)-(+)-citronellyl	• −19	• 47	• 63	•
37	phenyl–phenyl	C_3H_7	(S)-(+)-citronellyl	—	• 127	• 187	•
29	phenyl–phenyl	C_8H_{17}	(S)-(+)-citronellyl	—	• 97	• 132	•

ᵃParentheses denote a monotropic mesophase, * denotes a chiral nematic phase.

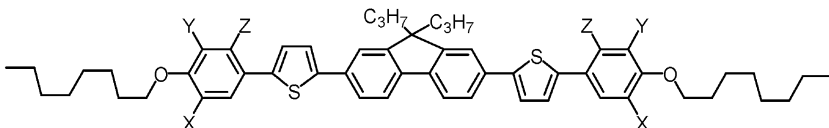Table 7.   Transition temperatures (°C) for the fluorenes **31**–**33**, **35**, **36** and **38**–**49**.

Compound	O*R*	*n*	g		Cr		N/N*		I
31		3	•	30	•	169	(•	168)[a]	•
38		3	•	32	•	153	(•	146)	•
39		3			•	222	(•	197)	•
40		3	•	45	•	194	(•	173)	•
41		3	•		•	174	(•	172)	•
42		3	(*R*) •	29	•	123	(•	122)	•
35		3	(*S*) •	23	•	123	(•	122)	•
43		3			•	110	•	124	•
44		3			•	60	•	83	•
32		8	•	−12	•	69	•	99	•
45		8	•	−12	•	59	•	71	•
36		8	(*S*) •	−19	•	47	•	63	•
46		3	(*S*)		•	58	•	87	•
47		8	(*S*) •	−13	•	62	(•	−3)	•
48		8	•	−4	•	72	(•	61)	•
49		8	•	−17	•	44	(•	16)	•

[a] Parentheses denote a monotropic mesophase.

to the absence of the rigid carbon–carbon double bonds and the subsequent increase in the flexibility of the C–C single bond. The two bulky methyl groups of the single bond can rotate relatively freely, but the restricted rotation of the double bond impairs movement of the bulky methyl groups. The effect on the clearing point is not as great, therefore the fluorene **43** exhibits an enantiotropic nematic phase at an elevated temperature compared with the monotropic nematic phase observed for compound **35**. Compound **48** exhibits a high melting point and a monotropic clearing point. The compound only crystallizes after several weeks standing and does not crystallize during repeated DSC heating and cooling cycles (down to −50°C), i.e. it exhibits a very high degree of supercooling over an extended time. Lower melting and clearing points are observed when the branched chain is increased and an additional branched methyl group is present in the chain of compounds **44** and **49**. This is due to the greater degree of flexibility of the longer branched alkyl chain and the increase in non-linear chain conformations. Also the additional

branched methyl group incorporated into the alkyl chain increases the steric effects between the chromophores, which also contribute to lowering of the melting and clearing points. The presence of a *cis*-double bond in fluorenes **38** and **45** reduces their melting and clearing points in comparison with the analogous fluorenes **31** and **32** with no *cis*-double bond in the terminal chain. These differences in the transition temperatures may occur because the presence of the *cis*-double bond is accompanied by a slight loss in linearity and accordingly a reduction in the length-to-breadth ratio [46]. Many of the fluorenes in table 7 exhibit a glass transition temperature.

The thermal data collated in table 8 show that the presence of lateral methyl substituents in compounds **50**–**52** results in much lower melting and clearing points than those of compound **31** without lateral substituents. Compound **50** exhibits the lowest melting and clearing points, in which mono-methyl substitution is directed *meta* to the ring junction. Unusually *ortho*-methyl substitution **52**, (which should lead to significant

Table 8. Transition temperatures (°C) for the fluorenes **31** and **50–52**.

Compound	X	Y	Z	g		Cr		N		I
31	H	H	H	•	30	•	169	(•	168)[a]	•
50	CH$_3$	H	H		—	•	111	(•	80)	•
51	CH$_3$	CH$_3$	H	•	26	•	120	(•	95)	•
52	H	H	CH$_3$	•	35	•	121	•	137	•

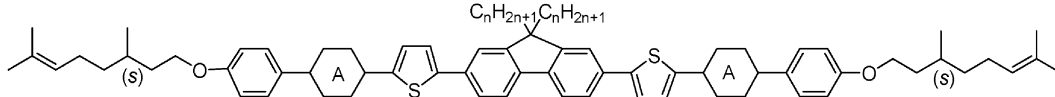[a]Parentheses denote a monotropic mesophase.

inter-annular twisting between the thiophene and benzene rings) is less effective than *meta*-substitution in reducing the transition temperatures. All three methyl-substituted derivatives **50–52** have similar melting points, which again demonstrates the imprecision in predicting the liquid crystal transition temperatures of even similar compounds.
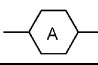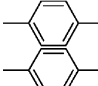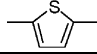
Compounds **53** and **54** are similar to compounds **35** and **36**, shown in table 7, in which the only difference is that two additional phenyl rings are incorporated into the aromatic core of **35** and **36**. All the melting points and clearing points of the compounds with eight aromatic rings shown in table 9 are higher than the melting and clearing points of the analogous compounds containing six aromatic rings. This is due to the greater length-to-breadth ratio and greater degree of conjugation. Extending the length-to-breadth ratio and the molecular weight can also increase the glass transition temperature of the material. Therefore, compounds **54** and **55** exhibit a higher T_g (10 and 29°C, respectively) compared with that (−19°C) of compound **36** that contains only six aromatic rings. This is possibly due to differences in viscosity. The presence of thiophene rings leads to a higher glass transition temperature; for example, the T_g of compound **55** is higher (+19°C) than that of compound **54**

which is identical apart from the replacement of a phenyl ring by a thiophene ring.

4. Conclusions

A wide range of light-emitting liquid crystals with different aromatic cores, lateral substituents and end groups has been successfully synthesized and their liquid crystalline phases and transition temperatures determined. A lowering of the melting point has been successfully achieved by varying the length of the alkyl chain at the 9-position of the fluorene core, by incorporating lateral substituents such as fluorine atoms and methyl groups, as well as by incorporating branched chains. These relationships can all be attributed to steric effects in one way or another. Compounds that incorporate thiophene and long alkyl chains at the fluorene 9-position tend to give rise to a glass transition often below room temperature. Higher T_g values can be obtained by decreasing the alkyl chain length at the 9-position of the fluorene core and by increasing the conjugation length. These compounds serve as useful models for the synthesis of luminescent analogous reactive mesogens having a nematic phase with a high clearing point and a melting point below room temperature.

Table 9. Transition temperatures (°C) for the fluorenes **53–55**.

Compound	n	A	g		Cr		N*		I
53	3			—	•	145	•	277	•
54	8		•	10	•	106	•	208	•
55	8		•	29	•	114	•	178	•

Acknowledgements

References

[1] C.D. Müller, A. Falcou, N. Reckefuss, M. Rojahn, V. Wiederhirn, P. Rudati, H. Frohne, O. Nuykens, H. Becker, K. Meerholz. *Nature*, **421**, 829 (2003).
[2] M. Grell, D.D.C. Bradley. *Adv. Mater.*, **11**, 895 (1999).
[3] A. Bacher, C.H. Erdelen, W. Paulus, H. Ringsdorf, H.-W. Schmidt, P. Schuhmacher. *Macromolecules*, **32**, 4551 (1999).
[4] A.E.A. Contoret, S. R Farrar, P.O. Jackson, L. May, M. O'Neill, J.E. Nicholls, G.J. Richards, S.M. Kelly. *Adv. Mater.*, **12**, 971 (2000).
[5] P. Strohriegel, D. Hanft, M. Jandke, T. Pfeuffer. *Mat. Res. Soc. Symp. Proc.*, **709**, 31 (2002).
[6] M. O'Neill, S.M. Kelly. *Adv. Mater.*, **15**, 1135 (2003).
[7] S.M. Kelly, M. O'Neill. In *Handbook of Electroluminescence*, D.R. Vij (Ed.), Chap. 14, IOP, and references therein (2004).
[8] M. O'Neill, S.M. Kelly. *Ekisho.*, **9**, 9 (2005).
[9] A.E.A. Contoret, M.P. Aldred, P. Vlachos, S. R Farrar, W.C. Tsoi, M. O'Neill, S.M. Kelly. *Adv. Mater.*, **17**, 1368 (2005).
[10] A. Bacher, P.G. Bentley, P. Glarvey, K.S. Whitehead, D.D.C. Bradley, M. Grell, M. Turner. *J. mater. Chem.*, **9**, 2985 (1999).
[11] A. Bacher, P.G. Bentley, D.D.C. Bradley, L.K. Douglas, P. Glarvey, M. Grell, K.S. Whitehead, M. Turner. *Synth. Met.*, **111–112**, 413 (2000).
[12] A.J. Eastwood, A.E.A. Contoret, S.R. Farrar, S. Fowler, S.M. Kelly, S.M. Khan, J.E. Nicholls, M. O'Neill. *Synth. Met*, **121**, 1659 (2001).
[13] A.E.A. Contoret, S.R. Farrar, P.O. Jackson, M. O'Neill, J.E. Nicholls, S.M. Kelly, G.J. Richards. *Synth. Met.*, **121**, 1645 (2001).
[14] A.E.A. Contoret, S.R. Farrar, M. O'Neill, J.E. Nicholls, G.J. Richards, S.M. Kelly, A.W. Hall. *Chem. Mater.*, **14**, 1477 (2002).
[15] M.P. Aldred, A.J. Eastwood, S.M. Kelly, P. Vlachos, B. Mansoor, M. O'Neill, W.C. Tsoi. *Chem. Mater.*, **16**, 4928 (2004).
[16] S. Méry, D. Haristoy, J.-F. Nicoud, D. Guillon, S. Diele, H. Monobe, Y. Shimizu. *J. mater. Chem.*, **12**, 37 (2002).
[17] M. Funahashi, J.-I. Hanna, *Appl. Phys. Lett.*, **73**, 3733 (1998); M. Funahashi, J.-I. Hanna. *Mol. Cryst. Liq. Cryst.*, **331**, 509 (1999); M. Funahashi, J.-I. Hanna. *Appl. Phys. Lett.*, **368**, 303 (2001); H. Maeda, M. Funahashi and J.-I. Hanna. *Mol. Cryst. liq. Cryst.*, **366**, 369 (2001).
[18] K. Kogo, H. Maeda, H. Kato, M. Funahashi, J.-I. Hanna. *Appl. Phys. Lett.*, **75**, 3348 (1999).
[19] M.G. Debije, Z. Chen, J. Piris, R.B. Neder, M.M. Watson, K. Müllen, F. Würthner. *J. mater. Chem.*, **15**, 1270 (2005).
[20] P. Vlachos, S.M. Kelly, B. Mansoor, M. O'Neill. *Chem.Commun.*, 1874 (2002).
[21] P. Vlachos, B. Mansoor, S.M. Kelly, M.P. Aldred, M. O'Neill. *Chem.Commun.*, 2921 (2005).
[22] I. McCulloch, W. Zhang, M. Heeney, C. Bailey, M. Giles, D. Graham, M. Shkunov, D. Sparrowe, S. Tierney. *J. mater. Chem.*, **13**, 2436 (2003).
[23] M. Millaruelo, L. Oriol, J.L. Serrano, M. Pinol, P.L. Sáez. *Mol. Cryst. liq. Cryst.*, **411**, 451 (2004).
[24] J. Barche, S. Janietz, M. Ahles, R. Schmechel, H. Seggern. *Chem. Mater.*, **16**, 4286 (2004).
[25] M.P. Aldred, P. Vlachos, D. Dong, S.P. Kitney, W.C. Tsoi, M. O'Neill, S.M. Kelly. *Liq. Cryst.*, **32**, 951 (2005).
[26] M.P. Aldred, M. Carrasco-Orozoco, A.E.A. Contoret, D. Dong, S.R. Farrar, S.M. Kelly, S.P. Kitney, D. Mathieson, M. O'Neill, W.C. Tsoi, P. Vlachos, K.L. Woon. *J. mater. Chem* (submitted).
[27] T. Tsutsui, C.P. Lin, S. Saito, S.H. Chen, H. Shi, J.C. Mastrangelo. *Mat. Res. Soc. Proc.*, **425**, 225 (1996).
[28] M. Jandke, D. Hanft, P. Strohriegel, K. Whitehead, M. Grell, D.D.C. Bradley. *Proc. SPIE*, **4105**, 338 (2001).
[29] S.W. Culligan, Y.H. Geng, S.H. Chen, K. Klubeck, K.M. Vaeth, C.W. Tang. *Adv. Mater.*, **15**, 1176 (2003).
[30] Y.H. Geng, S.W. Culligan, A. Trajkovska, J.U. Wallace, S.H. Chen. *Chem Mater.*, **15**, 542 (2003).
[31] J. Schmidtke, W. Stille, H. Finkelman, S.T. Kim. *Adv. Mater.*, **14**, 746 (2002).
[32] S.H. Chen, D. Katsis, A.W. Schmid, J.C. Mastrangelo, T. Tsutsui, T.N. Blanton. *Nature*, **397**, 506 (1999).
[33] K.L. Woon, M. O'Neill, G.J. Richards, M.P. Aldred, S.M. Kelly, A.M. Fox. *Adv. Mater.*, **15**, 1555 (2003).
[34] N. Miyaura, T. Yanagi, A. Suzuki. *Synth. Commun.*, **11**, 513 (1981).
[35] J.F. McOmie, M.L. Watts, D.E. West. *Tetrahedron*, **24**, 2289 (1968).
[36] H. Feuer, J. Hooz. In *The Chemistry of the Ether Linkage*, S. Patai (Ed.), p. 445, Wiley, New York (1967).
[37] J.K. Stille. *Angew. Chem. int. Ed.*, **25**, 508 (1986).
[38] M. Grell, D.D. C Bradley, E.P. Woo, M. Inbasekaran. *Adv. Mater.*, **10**, 9 (1997).
[39] D. Neher. *Macromol. rapid Commun.*, **22**, 1366 (2001).
[40] D. Sainova, A. Zen, H.G. Nothofer, U. Asawapirom, U. Scherf, R. Hagen, T. Bieringer, S. Kostromine, D. Neher. *Adv. func. Mater.*, **12**, 49 (2002).
[41] M. Ranger, M. Leclerc. *Macromolecules*, **32**, 3306 (1999).
[42] R. Güntner, T. Farrell, U. Scherf, T. Miteva, A. Yasuda, G. Nelles. *J. mater. Chem.*, **14**, 2622 (2004).
[43] G.W. Gray. *Advances in Liquid Crystals,* Vol. 2, Academic press, London, and references therein (1976).
[44] G. Tammann. *The State of Aggregation* 2 Edn, Van Nostrand, New York (1992).
[45] C.C. Wu, Y.T. Yin, K.T. Wong, R.T. Chen, Y. Y Chien. *Adv. Mater.*, **6**, 61 (2004).
[46] S.M. Kelly. *Liq. Cryst.*, **20**, 493 (1996).